ARTICLE IN PRESS

Available online at www.sciencedirect.com
SCIENCE DIRECT®

Journal of Structural Biology xxx (2005) xxx–xxx

Journal of Structural Biology

www.elsevier.com/locate/yjsbi

An all-atom model of the pore-like structure of hexameric VP40 from Ebola: Structural insights into the monomer–hexamer transition

Tam Luong Nguyen [a], Guy Schoehn [b,c,d], Winfried Weissenhorn [d], Ann R. Hermone [a], James C. Burnett [a], Rekha G. Panchal [a], Connor McGrath [a], Dan W. Zaharevitz [a], M. Javad Aman [e], Rick Gussio [a,*], Sina Bavari [f,*]

[a] *Target Structure-Based Drug Discovery Group, Developmental Therapeutics Program, SAIC, National Cancer Institute, Frederick, MD 21702, USA*
[b] *Institut de Biologie Structurale, 38042 Grenoble, France*
[c] *Laboratoire de Virologie Moléculaire et Structurale, Université Joseph Fourier, 38042 Grenoble, France*
[d] *European Molecular Biology Laboratory, 38042 Grenoble, France*
[e] *Clinical Research Management Inc., Frederick, MD 21702, USA*
[f] *US Army Medical Research Institute of Infectious Diseases, Fort Detrick, Frederick, MD 21702, USA*

Received 3 December 2004, and in revised form 17 February 2005

Abstract

The matrix protein VP40 is an indispensable component of viral assembly and budding by the Ebola virus. VP40 is a monomer in solution, but can fold into hexameric and octameric states, two oligomeric conformations that play central roles in the Ebola viral life cycle. While the X-ray structures of monomeric and octameric VP40 have been determined, the structure of hexameric VP40 has only been solved by three-dimensional electron microscopy (EM) to a resolution of ~30 Å. In this paper, we present the refinement of the EM reconstruction of truncated hexameric VP40 to ~20 Å and the construction of an all-atom model (residues 44–212) using the EM model at ~20 Å and the X-ray structure of monomeric VP40 as templates. The hexamer model suggests that the monomer–hexamer transition involves a conformational change in the N-terminal domain that is not evident during octamerization and therefore, may provide the basis for elucidating the biological function of VP40.
Published by Elsevier Inc.

Keywords: Oligomerization; Pore-like structure; Molecular modeling; Conformational change; β-sandwich; Electron microscopy

1. Introduction

The Ebola virus is a non-segmented, negative strand RNA virus that causes hemorrhagic fever in humans with a mortality rate exceeding 70% (Feldmann et al., 2003). The matrix protein VP40 is the most abundant protein in the Ebola virus, and plays significant structural and functional roles in the Ebola life cycle. Positioned beneath the viral membrane, VP40 may provide structural integrity to the viral particle by linking the membrane to the nucleocapsid (Feldmann and Klenk, 1996). In addition, VP40 plays a central role in viral assembly and budding (Aman et al., 2003; Bavari et al., 2002; Panchal et al., 2003; Timmins et al., 2004). VP40 binds and recruits specific human cellular proteins (Harty et al., 2000; Licata et al., 2003; Timmins et al., 2003b) to the budding site, allowing the virus to exploit cellular pathways in its assembly and vesicular release (Jasenosky et al., 2001; Timmins et al., 2001).

The X-ray structure of monomeric VP40 (PDB entry 1ES6, residues 44–321) has been determined to a

* Corresponding authors. Fax: +1 301 846 6106 (R. Gussio), +1 301 619 2348 (S. Bavari).
E-mail addresses: Gussio@ncifcrf.gov (R. Gussio), Sina.Bavari@amedd.army.mil (S. Bavari).

1047-8477/$ - see front matter. Published by Elsevier Inc.
doi:10.1016/j.jsb.2005.02.013

Report Documentation Page

Form Approved
OMB No. 0704-0188

1. REPORT DATE	2. REPORT TYPE	3. DATES COVERED
19 MAY 2005	**N/A**	**-**

4. TITLE AND SUBTITLE	5a. CONTRACT NUMBER
An all-atom model of the pore-like structure of hexameric VP40 from Ebola: structural insights into the monomer-hexamer transition, Journal of Structural Biology 19 (epub ahead of print)	5b. GRANT NUMBER
	5c. PROGRAM ELEMENT NUMBER
6. AUTHOR(S) **Nguyen, TL Schoehn, G Weissenhorn, W Hermone, AR Burnett, JC Panchal, RG McGrath, C Zaharevitz, DW Aman, MJ Gussio, R Bavari, S**	5d. PROJECT NUMBER
	5e. TASK NUMBER
	5f. WORK UNIT NUMBER
7. PERFORMING ORGANIZATION NAME(S) AND ADDRESS(ES) **United States Army Medical Research Institute of Infectious Diseases, Fort Detrick, Frederick, MD**	8. PERFORMING ORGANIZATION REPORT NUMBER **RPP-04-350**
9. SPONSORING/MONITORING AGENCY NAME(S) AND ADDRESS(ES)	10. SPONSOR/MONITOR'S ACRONYM(S)
	11. SPONSOR/MONITOR'S REPORT NUMBER(S)

12. DISTRIBUTION/AVAILABILITY STATEMENT
Approved for public release, distribution unlimited

13. SUPPLEMENTARY NOTES
The original document contains color images.

14. ABSTRACT
The matrix protein VP40 is an indispensable component of viral assembly and budding by the Ebola virus. VP40 is a monomer in solution, but can fold into hexameric and octameric states, two oligomeric conformations that play central roles in the Ebola viral life cycle. While the X-ray structures of monomeric and octameric VP40 have been determined, the structure of hexameric VP40 has only been solved by three-dimensional electron microscopy (EM) to a resolution of approximately 30A. In this paper, we present the refinement of the EM reconstruction of truncated hexameric VP40 to approximately 20A and the construction of an all-atom model (residues 44-212) using the EM model at approximately 20A and the X-ray structure of monomeric VP40 as templates. The hexamer model suggests that the monomer-hexamer transition involves a conformational change in the N-terminal domain that is not evident during octamerization and therefore, may provide the basis for elucidating the biological function of VP40.

15. SUBJECT TERMS
filovirus, Ebola, model, structure

16. SECURITY CLASSIFICATION OF:			17. LIMITATION OF ABSTRACT	18. NUMBER OF PAGES	19a. NAME OF RESPONSIBLE PERSON
a. REPORT	b. ABSTRACT	c. THIS PAGE			
unclassified	**unclassified**	**unclassified**	**SAR**	**11**	

resolution of 2.0 Å and reveals that VP40 consists of structurally homologous N- and C-terminal domains (Dessen et al., 2000). The two domains are folded into similar β-sandwiches composed of two β-sheets of three antiparallel strands with three α-helices packed laterally to each β-sandwich (Fig. 1A). The two domains are oriented at an angle of 60° to one another, are linked by a large flexible loop, and are loosely associated. In contrast to their structural similarity, the N- and C-terminal domains have distinct biological roles. The N-terminal domain is central to oligomerization and the C-terminal domain to membrane-binding (Panchal et al., 2003; Ruigrok et al., 2000; Scianimanico et al., 2000).

While it exists as a monomer in solution, VP40 can also fold into hexameric and octameric states, when treated with urea, bound to liposomes or truncated at its C-terminus (Ruigrok et al., 2000; Scianimanico et al., 2000; Timmins et al., 2003a). The X-ray structure of octameric VP40 has been determined to a resolution of 1.6 Å and shows a pore-like structure composed of four antiparallel dimers complexed with short RNA strands (triribonucleotide 5′-U-G-A-3′) (PDB entry 1H2D, residues 69–191(192)) (Gomis-Ruth et al., 2003) (Fig. 1B). With the eight RNA segments bound at the dimer–dimer interfaces, the pore-like structure of octameric VP40 has an inside diameter of 17 Å (~30 Å in the absence of the RNA strands), an outside diameter of 84 Å, and a height of 42 Å (Fig. 1C). Based upon analyses of the monomeric and octameric VP40 X-ray structures, it is apparent that the monomer–octamer transition involves: (1) the unfolding of the N-terminal segment and (2) a conformational switch of the N- and C-terminal domains, in which the C- terminal domain moves to open up the oligomerization interface.

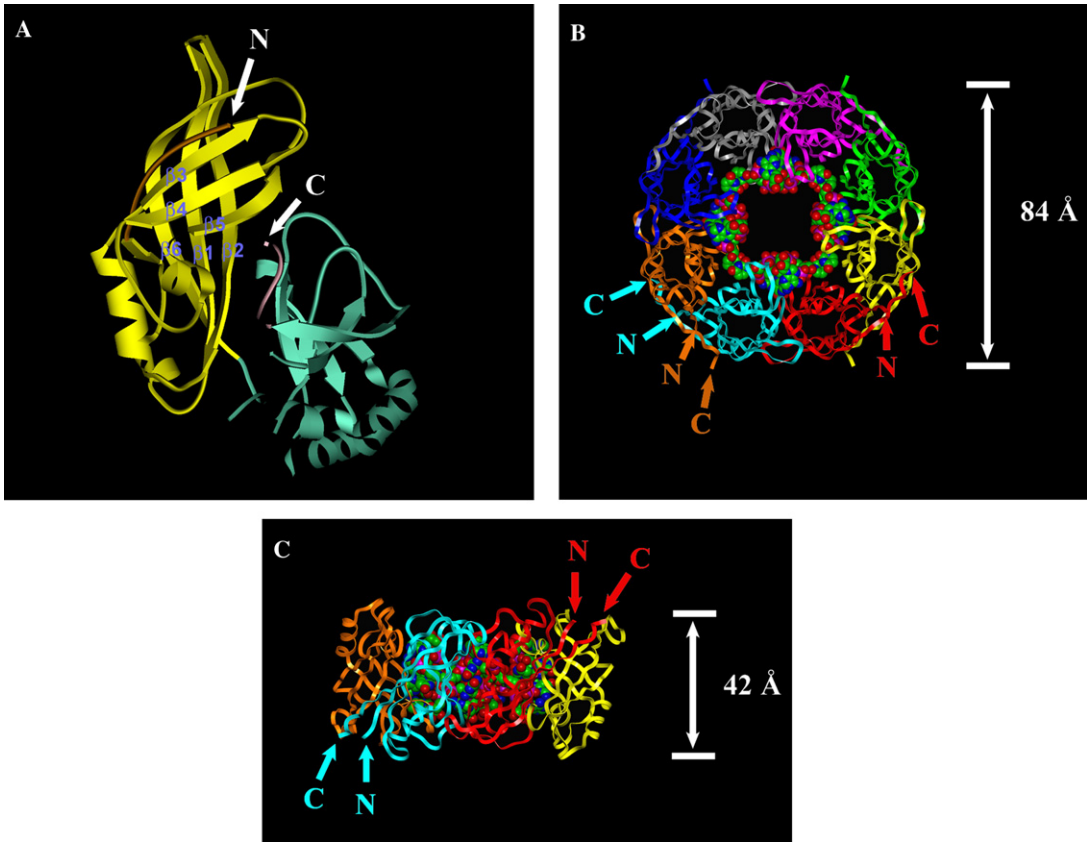

Fig. 1. X-ray structures of monomeric and octameric VP40. (A) In the X-ray structure of monomeric VP40 (31–212), the N- and C-terminal domains are colored yellow and green, respectively. The N- and C-terminal loops are labeled and colored orange and purple, respectively, to highlight their relative positions. The N- and C-terminal domains are unlinked because residues 195–200 were untraceable in the X-ray structure. Furthermore, the N-terminal segment (residues 31–43) was not located on the electron density map, presumably because of its conformational flexibility. The dimensions of the structure are 40 × 50 × 25 Å. (B and C) The X-ray structure of octameric VP40 (69–194) is complexed with eight short RNA single strands (triribonucleotide 5′-U-G-A-3′). The eight VP40 subunits are rendered in ribbon and are colored coded. The eight RNA strands are drawn as CPK models with the carbon atoms colored green, nitrogen atoms blue, oxygen atoms red, and phosphorous atoms purple. (B) The N- and C-termini for one antiparallel dimer (orange and cyan ribbon) are labeled as well as one adjacent subunit (red ribbon). The pore-like structure of octameric VP40 has an outside diameter of 84 Å and an inside diameter of 17 Å in the presence of RNA and of 30 Å in the absence of RNA. (C) The N- and C-termini for the subunits forming a dimer–dimer interface (cyan and red ribbon) are labeled. A side view shows that the pore-like structure of octameric VP40 has a height of 42 Å. For clarity, only four of the eight VP40 subunits are shown.

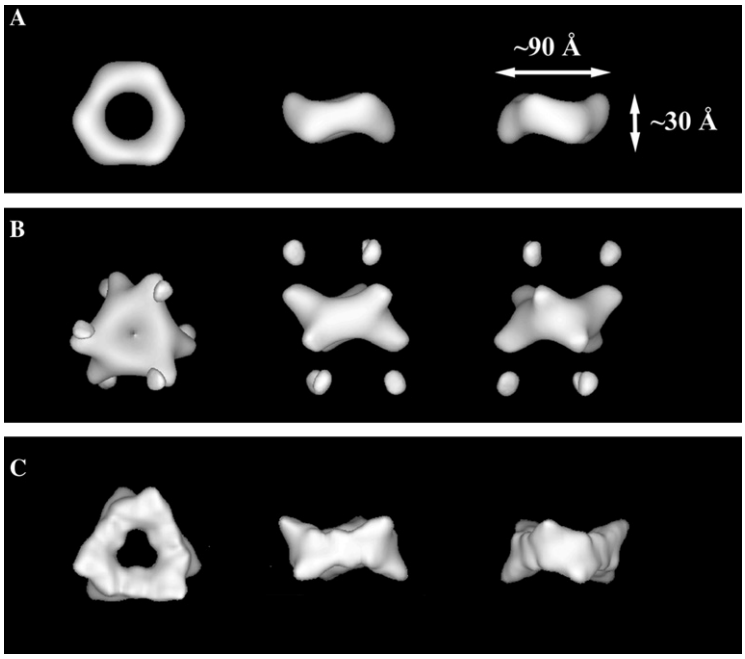

Fig. 2. EM reconstruction of truncated (31–212) and full-length (31–326) VP40. The left column shows that top view of each EM reconstruction, the middle column was obtained by a 90° rotation of the top view along the *x*-axis, and the right column is a 60° rotation of the middle column along the *y*-axis. (A) The EM reconstruction of truncated hexameric VP40 at a resolution of ~30 Å reveals a pore-like structure formed by the oligomerization of the N-terminal domain. The pore-like structure has an outside diameter of ~90 Å, an inside diameter of ~30 Å, and a height of ~30 Å. The homodimers that comprise the pore-like structure have a width of 55 Å (adapted from Ruigrok et al., 2000). (B) The EM reconstruction of the nearly full-length hexameric VP40 refined to ~30 Å shows that the C-terminal domain alternates between positions above and below the pore-like structure. The C-terminal domain is responsible for membrane-binding. The lower electron density of the C-terminal domains relative to the N-terminal domains suggests that the C-terminal domains are conformationally flexible (adapted from Scianimanico et al., 2000). (C) The EM reconstruction of truncated hexameric VP40 refined to ~20 Å shows the surface features of the pore-like structure in greater detail. The donut-like shape of hexameric VP40 at ~30 Å decomposes to two triangles offset by ~30°. Additionally, the circular channel at ~30 Å becomes a cloverleaf shape at ~20 Å. The side view of the pore-like structure shows a chair-like conformation.

Recent mutagenesis data indicate that octameric VP40 is essential for the Ebola virus life cycle (Hoenen et al., 2005).

At present, the atomic structure of hexameric VP40 has not been determined. However, previous structural studies of hexameric VP40 using electron microscopy have resulted in the three-dimensional reconstruction of truncated (residues 31–212) and nearly full-length (residues 31–326) hexameric VP40 refined to ~30 Å (Figs. 2A and B) (Ruigrok et al., 2000; Scianimanico et al., 2000). Similar to octameric VP40, hexameric VP40 has a pore-like structure. From these reconstructions, it is apparent that hexameric VP40 is a trimer of antiparallel dimers, in which the N-terminal domains form a pore-like structure and the C-terminal domains alternate between positions above and below the pore-like structure. The lower electron density of the C-terminal domains relative to the N-terminal domains suggests that the C-terminal domains are conformationally flexible. One would expect that since hexameric VP40 consists of fewer N-terminal domains than octameric VP40, its pore-like structure would have a smaller outside diameter than that of octameric VP40, assuming a similar conformation and orientation of the N-terminal domains in the two oligomeric states. However, the pore-like structure of hexameric VP40 has an outside diameter of ~90 Å and an inside diameter of 30–35 Å, which are the approximate diameters of octameric VP40. Furthermore, the pore-like structure of hexameric VP40 has a height of ~30 Å, with each antiparallel dimer having a width of ~55 Å. The similar outside diameters of hexameric and octameric VP40 indicate that there exist major structural differences between the N-terminal domains of the two oligomeric states. Unfortunately, because the atomic structure of hexameric VP40 has not been determined, these differences cannot be delineated.

As hexameric VP40 appears to be crucial to viral assembly and budding, determining its molecular structure is of great interest. Here, we present two models of hexameric VP40, a three-dimensional EM reconstruction of truncated hexameric VP40 at ~20 Å (31–212) which was used in the model building and the all-atom model of hexameric VP40 (44–212). The model was built using the N-terminal domain from the monomeric VP40 crystal structure as the initial structure and was fitted to the EM map of truncated hexameric VP40 at ~20 Å. The two structures and the conformational changes associated with hexamerization are discussed herein.

2. Materials and methods

2.1. General methods

A Silicon Graphics Octane 2 workstation with Insight II (Accelrys, San Diego, CA) was used to build and visualize the models. All simulations were performed using the Discover 3.0 program (Accelrys, San Diego, CA) with the molecular mechanics potentials set to the amber force field and the non-bonded interaction limited to 13 Å. The tethered minimization and constrained molecular dynamics protocols used to construct the hexameric VP40 model were previously described (Nguyen, 2004). The quality of the models was assessed using Procheck (Laskowski et al., 1993) and HINT (eduSoft, Richmond, VA). The root mean square deviation (r.m.s. deviation) values were calculated relative to the mean structure using MOLMOL (Koradi et al., 1996), and the figures were rendered using Molscript (Kraulis, 1991), Pymol (DeLano Scientific, San Carlos, CA), and Insight II.

2.2. EM model and fit

The EM model was recalculated from previous data with the same projection matching method as in Ruigrok et al. (2000) but by correcting the images for the contrast transfer function (CTF) according to the Conway and Steven (1999) method. The resolution of the final map is ~20 Å, as tested by Fourier shell correlation. The fit between the EM map and the molecular model was performed manually using O, and the result was then submitted to Situs (Wriggers and Birmanns, 2001), which gave a correlation of 0.208.

2.3. All-atom model

Fig. 3 outlines the protocol used to generate the all-atom model. The initial structure is the monomeric VP40 crystal structure, which consists of the N- and C-terminal domains. Residues 213–321 of the C-terminal domain were removed. The result is a truncated N-terminal domain (residues 44–212). Using the Cα trace of the β-sandwiches as guides, two copies of the truncated monomeric form of the N-terminal domain were manually superimposed onto the antiparallel dimer of the octameric VP40 crystal structure. The protomer–protomer interface was both energetically and hydropathically refined. This involved: (1) manual adjustment of the torsion angles of the side chains at the protomer–protomer interface to relieve van der Waals violations of greater than 0.25 Å, (2) energy minimization involving up to 5000 steps of Fletcher–Powell optimization until the norm of the gradient was <1.0 kcal/mol Å^2. During this energy minimization, the backbone atoms of the two protomers were fixed in Cartesian space so that the overall structure of the complex was maintained, (3) hydropathic analysis of the refined protomer–protomer interface using the HINT program and comparison to the hydropathic quality of the octameric VP40 crystal structure, and (4) constrained energy minimization in which unfavorable hydrophobic–polar and basic–basic interactions as defined by HINT values higher than those in the octameric VP40 crystal structure were relieved by distance constraints which incrementally separated the atoms involved in the unfavorable interaction.

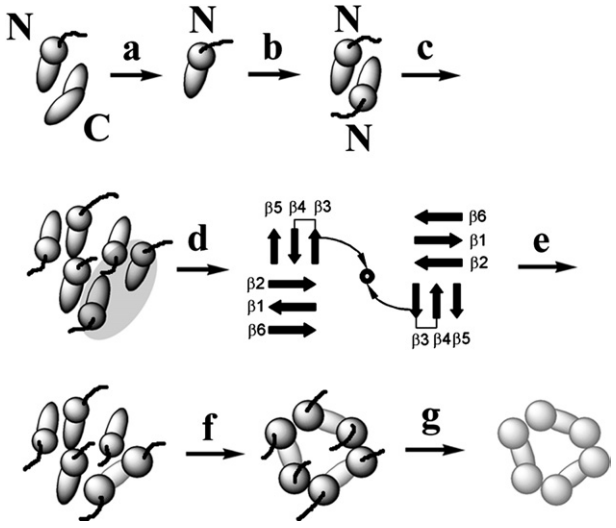

Fig. 3. Schematic detailing the methodology used to model the hexameric VP40 structure. The initial structure is the X-ray structure of monomeric VP40 (44–321), which consists of the two structurally homologous N- and C-terminal domains. (a) Residues of the C-terminal domain (213–321) are removed and residues which were missing in the N-terminal domain were modeled to produce a N-terminal domain with a sequence of 44–212. (b) Using the antiparallel dimers of the octameric VP40 crystal structure as a template, two copies of the modeled N-terminal domain were dimerized in an antiparallel fashion. The protein–protein interface was refined to the hydropathic quality evident in the octameric VP40 crystal structure. (c) Using the volume and dimensions of the EM reconstruction of hexameric VP40 as restraints, three copies of the model VP40 dimer were positioned into a hexameric assembly. (d) Because there are large gaps in the dimer–dimer interfaces, it was necessary to use constrained molecular dynamics to produce tightly packed protein–protein surfaces. This mostly involved the rigid-body shift of the β-sheet consisting of strands β3, β4, and β5 towards the center of the protein–protein gap. One dimer–dimer interface is refined. (e and f) Instead of modeling the conformational change at the two remaining dimer–dimer interfaces, the two subunits of the refined dimer–dimer interface are hexamerized. The protomer–protomer interfaces are energetically and hydropathically refined. (g) The C-terminal loop residues which were in the nearly extended conformation in the monomeric VP40 crystal structure are packed using energy minimization and constrained molecular dynamics to produce the final model.

Initially, three of the modeled antiparallel dimers were arrayed into a ring-like structure with a diameter of ~90 Å. Because of their size and shape, the antiparallel dimers in this initial ring-like structure were not tightly packed, but were separated by ~15 Å gaps, as measured between Cα atoms. The protomers were rotated in a rigid-body fashion in an attempt to close these large protein–protein gaps. However, this approach was unsuc-

cessful. Structural analyses indicated that closing these large gaps required a major conformational change in the sheet structure formed by strands β3, β4, and β5. If these strands from each protomer were moved in a concerted fashion towards the opening at the center of the dimer–dimer interface and were packed against one another in an energetically and hydropathically reasonable manner, the result would be a pore-like structure with an outside diameter of ~90 Å and an inside diameter of ~30 Å. Absent this conformational change in the tertiary structure of VP40, the large gaps at the dimer–dimer interfaces could be closed by the rigid-body translation of the three antiparallel dimers towards the center of the ring-like structure. However, this would produce a ring-like structure with an outside diameter of only ~70 Å and lacking a channel (data not shown).

A constrained molecular dynamics protocol was used to produce the necessary conformational changes in strands β3, β4, and β5. Since the antiparallel dimers in hexameric VP40 are related by a threefold rotational axis, an efficient molecular design strategy and the one which was used here is to close the spatial gap at one dimer–dimer interface and then to copy the closed dimer–dimer subunit to the other two positions to form the closed hexamer. Because the hexamer must be reassembled from different dimer–dimer subunits, it was necessary to fix the positions of some of the atoms of the dimer–dimer subunits during molecular dynamics in order to properly reassemble the hexamer. We chose to fix the peptide backbone of strands β1, β2, and β6, since this prevents unnecessary translation or rotation of the protomers and additionally maintains the structural integrity of the protomer–protomer interfaces. During the simulations, distance constraints were used to maintain the secondary structure of the protein and allowed strands β3, β4, and β5 to move as a single unit. Two protomers at a dimer–dimer interface were selected and a methane molecule was positioned near the center of the dimer–dimer interface but outside of the ring-like structure. Distance constraints were created between the methane carbon and the Lys127 Cα atoms of the two protomers at the dimer–dimer interface. During the molecular dynamics simulations, the upper limits of these distance constraints were incrementally decreased to bring the two Lys127 Cα atoms closer to the methane molecule, and consequently, the two sheet structures towards the center of the dimer–dimer interface. Once the two sheet structures were brought within van der Waals contact distance to one another, tethered minimization, molecular dynamics, and torsional angle adjustments were used to energetically and hydropathically optimize the protein–protein interactions.

Using the initial ring-like structure as a template, three of the modeled dimer–dimer subunits were arrayed into a hexamer. With the peptide backbone of strands β1, β2, and β6 no longer fixed in Cartesian space, the protomer–protomer interfaces in the above hexameric structure were refined using tethered minimization, molecular dynamics, and torsional adjustment. In the final stage, residues 187–212, which are part of the large flexible loop connecting the N- and C-terminal domains, were folded using constrained molecular dynamics and positioned near the outside corners of the pore-like structure. The quality of the model was assessed using Procheck, which showed 98.3% of the residues in the most favored or additionally allowed regions.

3. Results and discussion

3.1. EM map refined to ~20 Å

The three-dimensional EM reconstruction of truncated and full-length hexameric VP40 had previously been reported at ~30 Å (Ruigrok et al., 2000; Scianimanico et al., 2000). Both EM reconstructions show that the pore-like structure of hexameric VP40 has a donut-like shape with a circular channel and rounded edges (Figs. 2A and B), which from the side view, has a chair-like conformation. Here, refinement of the EM map of truncated hexameric VP40 to ~20 Å reveals some important structural characteristics. First, the donut-like structure evident in the top view at ~30 Å decomposes into two triangular structures at ~20 Å (Fig. 2C). The two triangles are offset from one another by ~30° relative to the channel axis. Second, at the higher resolution, the channel of hexameric VP40 adopts a cloverleaf-like shape (Fig. 2C). The protomer–protomer interfaces outline the three leaves of the cloverleaf shape, while the dimer–dimer interfaces form the bulges in the channel. The side view of the EM reconstruction shows a similar chair conformation at ~20 Å and at ~30 Å. As evident in Fig. 2, more of the structural details of hexameric VP40 are revealed at ~20 Å and these features were incorporated into the model building.

3.2. Overall structure of the hexamer model

As shown in Fig. 4, the overall structure of the hexamer model is strikingly similar to the EM reconstruction at ~20 Å. Consistent with EM reconstructions, the atomic model has an outside diameter of 90 Å, an inside diameter of 30–35 Å, and a height of 30–40 Å. The height decreases to 30 Å near the dimer–dimer interface with the dimers having a width of ~55 Å. Besides their similar dimensions, the hexamer model features a channel with the distinctive cloverleaf shape evident in the EM maps at ~20 Å. As expected, while the leaves of the cloverleaf are shaped by the protomer–protomer interface, the bulges in the channel are formed by the dimer–dimer interfaces. The surface potential at the top of the hexamer model is mostly acidic near the protomer–protomer interfaces and basic near the dimer-dimer interfaces (Fig. 4A). From the side view, the

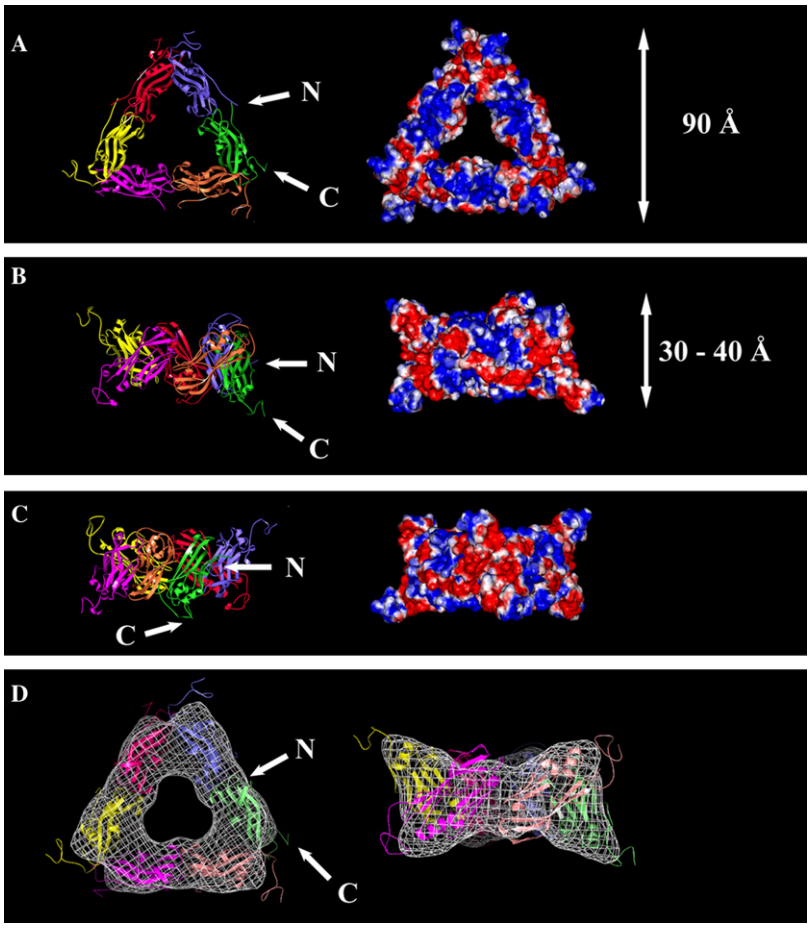

Fig. 4. Molecular model of truncated hexameric VP40 (44–212) and its fit to the EM map. The hexamer model is rendered in ribbon and the protomers are colored coded. The N- and C-termini are shown for one subunit (rendered in green). Surface renderings are colored according to the negative (red) and positive (blue) electrostatic surface potential. (A) The top view shows that the hexamer model has a triangular shape with an outside diameter of 90 Å and an inside diameter of ~30 Å. The dimer–dimer interfaces are mostly basic and the protomer–protomer interfaces are mostly acidic. The cloverleaf shape of the channel is also evident. (B) A 90° rotation along the *x*-axis of the top view shows that the model has a height of 30–40 Å. The height varies and narrows to ~30 Å at the dimer–dimer interfaces. Near the dimer–dimer interfaces, there are both positive and negative charge surfaces. (C) A 60° rotation along the *y*-axis of (B) shows that the protomer–protomer interfaces are mostly acidic. (D) The hexamer model is fitted to the EM map at ~20 Å, resulting in a coefficient of 0.208. The top view shows that the model has the triangular shape of the EM reconstruction as well as the cloverleaf-like channel. The side view (a 90° rotation along the *x*-axis) shows the chair-like conformation of hexameric VP40. While much of the hexamer model fits into the EM map, the C-terminal residues 190–212 are outside of the electron density. Residues 190–212 form the large flexible loop connecting the N- and C-terminal domains and, therefore, are highly disordered.

surface potential is both positive and negative at the dimer–dimer interfaces (Fig. 4B), but mostly negative at the protomer–protomer interfaces (Fig. 4C).

Each protomer in the hexamer model is composed of two β-sheets consisting of three antiparallel strands and three α-helices. A similar secondary structure is evident for the monomeric and the octameric states of the N-terminal domain. As a consequence of the approach used to generate the model, the protomers of the model are not identical, but have a r.m.s. deviation of ~1 Å for the backbone atoms of residues 44–194.

3.3. Docking of the model into the EM map

To validate the hexamer model, it was docked into the EM map of truncated hexameric VP40 at ~20 Å. The result was a correlation of 0.208. Fig. 4D shows that while much of the hexamer model fits into the EM map at ~20 Å, the C-terminal segments (residues 190–212) of the hexamer model are outside of the electron density. Residues 190–212 form the large loop connecting the N- and C-terminal domains in monomeric VP40 and are highly disordered, as indicated by the fact that residues 195–200 were untraceable in the monomeric VP40 X-ray structure. Because of their conformational flexibility, residues 190–212 may not be detectable in the EM images. Similarly, the N-terminus may be highly disordered (residues 31–43 were not located in the electron density map of monomeric VP40) and not visible by EM. Although it is clear that the unfolding of the N-terminal segment is a critical step in VP40 oligomerization, there is little structural information to suggest the conforma-

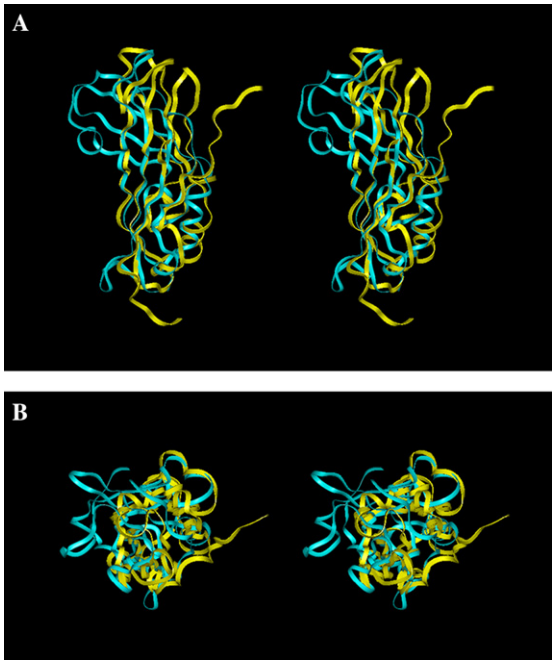

Fig. 5. Stereoview of the superimposition of the calculated average protomer of the hexamer model (44–194) and the N-terminal domain of the monomeric VP40 X-ray structure (44–194). The average protomer of the hexamer model is rendered in yellow ribbon and the monomer crystal structure in cyan ribbon. The two structures were superimposed along the Cα trace of strands β1, β2, and β6. (A) While much of the two structures can be overlapped, there are considerable differences between the two, particularly for strands β3, β4, and β5 which form a three-stranded β-sheet. (B) A rotation of 90° along the *x*-axis shows the top view of the superimposition and illustrates the different conformational space occupied by the N-terminal domains of the hexamer model and the monomer crystal structure.

tion and position of the N-terminal segments in hexameric VP40. Accordingly, while the construct used in the EM studies consisted of residues 31–212, residues 31–43 were not included in the hexameric VP40 model. The N-terminal segments of the hexameric VP40 model were positioned at the dimer–dimer interface and on the outside of the pore-like structure (Fig. 4C). Finally, the ring interior of the hexamer model has more of a triskelion appearance. This could easily be due to the use of stain that induces a Fresnel fringe at the inside of the particle.

3.4. Comparison to the monomeric VP40 X-ray structure

The N-terminal domains of the hexamer model and of the monomeric VP40 crystal structure possess the same secondary structural elements, but have distinct tertiary structures. Figs. 5A and B show the superimposition of the N-terminal domain (residues 44–194) from the X-ray structure of monomeric VP40 and the calculated average protomer from the hexamer model. The superimposition shows that while the two N-terminal domains occupy some common conformational space, major structural differences exist between the two.

Based on the superposition of strands β1, β2, and β6, the two structures have a backbone r.m.s. deviation of 2.9 Å for residues 44–194 (Fig. 6). This relatively low r.m.s. deviation value belies the major conformational changes in the N-terminal domain as a result of hexamerization. While strands β1, β2, and β6, which form one antiparallel β-sheet in the N-terminal domain, have an average backbone r.m.s. deviation of only 0.6 Å, strands β3, β4, and β5, which make up the second β-sheet structure in the N-terminal domain, have an average backbone r.m.s. deviation of 4.6 Å. The significantly higher r.m.s. deviation of strands β3, β4, and β5 is not unexpected, given that these strands were used to close the protein–protein gaps during model building. Because of the modeling methodology used to build the hexameric VP40 model, the turn residues 127–129 underwent the largest conformational changes and have

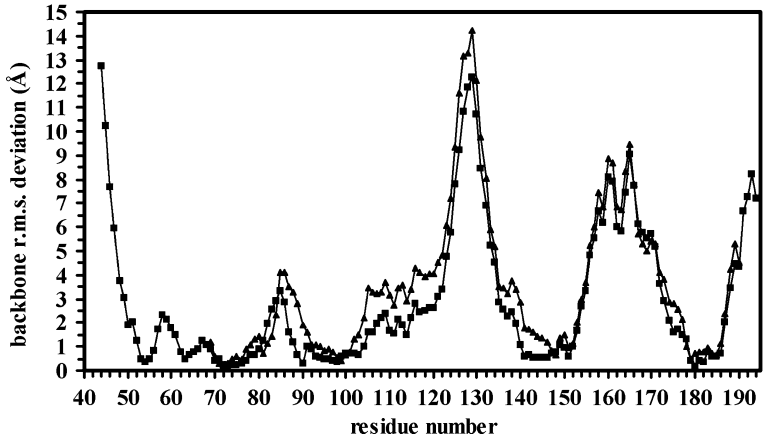

Fig. 6. Backbone r.m.s. deviation values of the calculated average protomer of the hexamer model compared to the N-terminal domains in the X-ray structures of monomeric (44–194) and octameric VP40 (69–191). The squares (■) depict the r.m.s. deviation values between the calculated average hexamer protomer and monomeric form of the N-terminal domain and the triangles (▲) between the calculated average hexamer protomer and the octameric state of the N-terminal domain. Because the monomeric and octameric states of the N-terminal domain are structurally similar, the two sets of r.m.s. deviation values parallel one another. The highest r.m.s. deviation values are observed for residues 127–129, which form a turn connecting strands β3 and β4.

an average r.m.s. deviation value of 11.6 Å. The model suggests that the monomer–hexamer transition involves a shift in two β-sheet structures of the N-terminal domain. As a measure of this shift, the centers of the two β-sheets move from a separation of 14.3 Å in the monomeric VP40 crystal structure to 16.6 Å in the hexamer model, a translation of 2.3 Å.

3.5. Comparison to the octameric VP40 X-ray structure

Although hexameric VP40 consists of fewer subunits than octameric VP40, the pore-like structures of the hexameric VP40 model and the octameric VP40 crystal structure have similar outside diameters of 90 and 84 Å, respectively, an indication that the N-terminal domains that make up the two pore-like structure have different conformations. Fig. 7 shows a side-by-side view of the antiparallel dimers from the hexamer model and the octamer X-ray structure. While consisting of similar secondary structures, the tertiary structures of the two dimers are strikingly different. As illustrated in Fig. 7B, the antiparallel dimer of the hexamer model has a more open structure than that of the octamer.

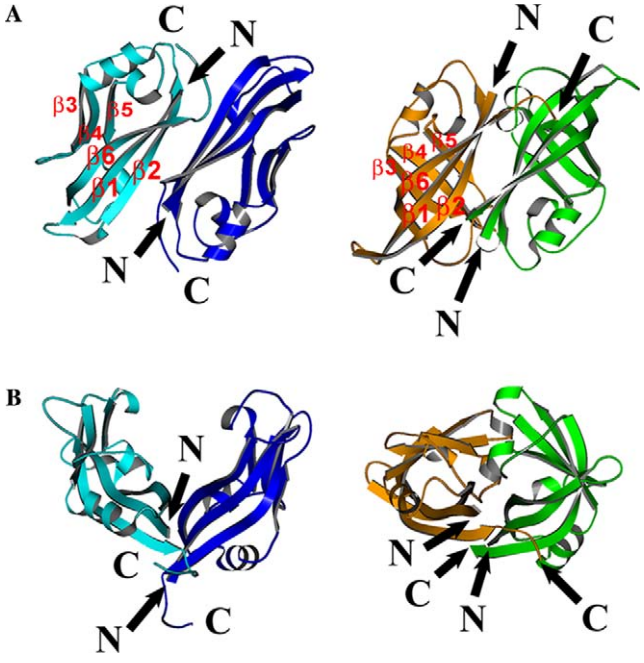

Fig. 7. Structural comparison of the antiparallel dimers in the hexameric VP40 model (residues 70–190) and in the octameric VP40 X-ray structure (70–190). Both dimers are rendered in ribbon. The two subunits of the antiparallel dimer in the hexamer model are colored blue and cyan (left), while those of the octamer crystal structure are colored green and orange (right). The two dimers are positioned with a similar orientation and illustrated side-by-side. The sheet structures in one subunit of the hexamer model and in one subunit of the octamer crystal structure are labeled. (A) While consisting of similar secondary structure, the tertiary structures of the two dimers are markedly different. (B) A 90° rotation of the two structures along the *x*-axis shows that the dimer from the hexamer model is a more open structure.

Based on the superimposition of strands β1, β2, and β6, subunit A of the octameric VP40 crystal structure and the calculated average protomer of the hexamer model have a backbone r.m.s. deviation of 3.5 Å for residues 69–190 (Fig. 6). Additionally, there are large differences in the β-sandwich structures of the hexamer model and octamer crystal structure. While the β-sheet formed by strands β1, β2, and β6 has an average r.m.s. deviation of 0.9 Å, the second β-sheet composed of strands β3, β4, and β5 has an average value of 5.6 Å. Similar to the monomer–hexamer comparison, the highest values are observed for residues 127–129 which form a turn connecting strands β3 and β4. In the octameric VP40 crystal structure, residues 127–129 are not hydrogen bonded and are positioned near the center of the channel. In contrast, the hexamer model suggests that the 127–129 loop is positioned at the dimer–dimer interface in hexameric VP40. These r.m.s. deviation values indicate that the two β-sheets in VP40 move farther apart during hexamerization than during octamerization. In the octamer X-ray structure and the hexamer model, the centers of the two β-sheets are separated by 14.7 and 16.6 Å, respectively.

3.6. Comparison of the protein–protein interfaces

Because the boundaries between the VP40 subunits in the EM reconstructions are not well defined, the features of the protein–protein interfaces in hexameric VP40 are largely unknown. By providing atomic detail to the EM reconstructions, the hexamer model suggests potential interactions at the protein–protein interfaces and may provide the basis for future work.

There are two types of protein–protein interfaces in the hexamer model and the octamer crystal structure. The first, the protomer–protomer interface, reflects the contacts formed between the protomers within the dimers of the two oligomeric conformations of VP40, while the second, the dimer–dimer interface, reflects the interactions between dimers. The hexamer model suggests that hexameric and octameric VP40 have similar protomer–protomer interfaces and strikingly different dimer–dimer interfaces.

In the octameric VP40 crystal structure, hydrophobic contacts dominate the protomer–protomer interfaces with Ile74, Trp95, Pro97, Phe161, and Ile182 forming a hydrophobic core. Similarly, in the hexamer model, hydrophobic contacts comprised of Ile74, Trp95, Pro97, and Ile182 appear to stabilize the protomer–protomer interfaces (Fig. 8A). Additionally, in octameric VP40, this hydrophobic core is complemented by salt bridge interactions from Glu160 to Arg148 and Arg151. The hexamer model suggests that this Arg148-Glu160 salt bridge is replaced by a cation–π interaction (Flocco and Mowbray, 1994; Mitchell et al., 1994) between the ring of Trp95 and the guanidinium group of Arg148 from neighboring subunits of hexameric VP40.

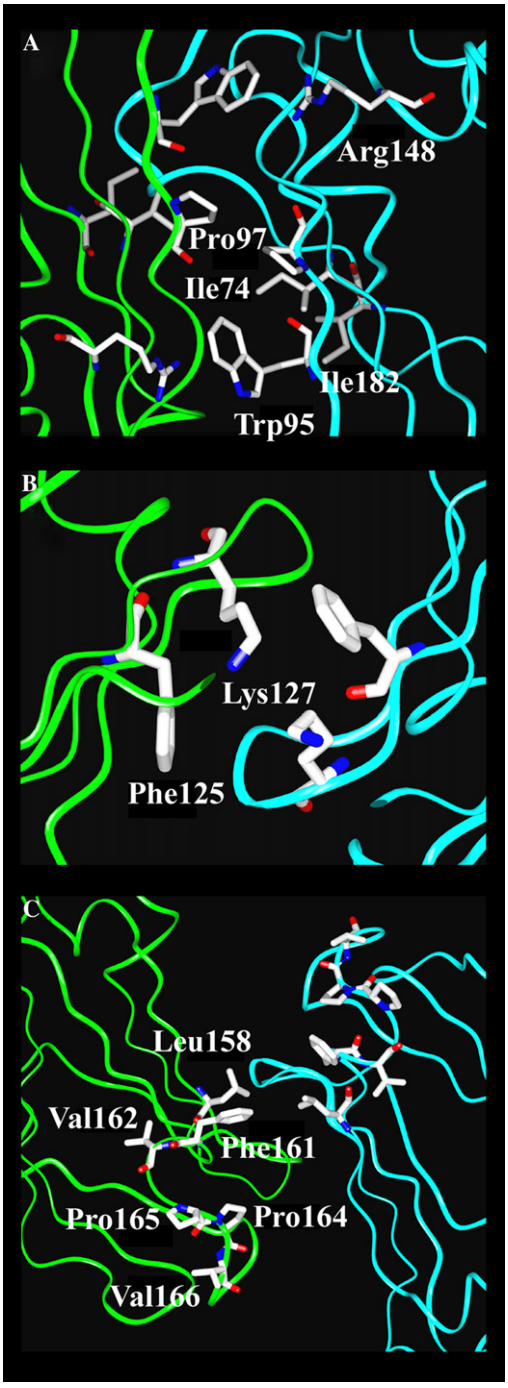

Fig. 8. Notable interactions at the protein–protein interfaces in the hexamer model. The two interface subunits are rendered as ribbon and colored either green or cyan. The identified residues are rendered in sticks with the carbon atoms colored white, the nitrogen atoms blue, and the oxygen atoms red. (A) The protomer–protomer interface is dominated by hydrophobic contacts. Ile74, Trp95, Pro97, and Ile182 form a hydrophobic core. Complementing this hydrophobic core is a cation–π interaction between Trp95 and Arg148 of the neighboring subunit. (B) The dimer–dimer interfaces also feature a cation–π interaction, but in this instance between Phe125 and Lys127. (C) The bulges evident in the channel interior of the model and the EM reconstruction of truncated hexameric VP40 at 20 Å occur at the dimer–dimer interfaces and are mostly hydrophobic, consisting of Leu158, Phe161, Val162, Pro164, Pro165, and Val166.

The hexamer model suggests that hydrophobic residues are critical to the stability of the dimer–dimer interfaces in hexameric VP40 with the aromatic ring of Phe125 playing a central role. In addition to providing hydrophobic contacts, the ring of Phe125 forms a cation–π interaction with the side chain amino group of Lys127 (Fig. 8B). In addition, clusters of hydrophobic residues line the channel interior at the dimer–dimer interfaces. These clusters form the three bulges which are evident in the EM reconstruction at ~20 Å and are responsible for the cloverleaf-like shape of the channel. Leu132, Phe157, Leu158, Phe161, Val162, Pro164, Pro165, and Val166 comprise these clusters (Fig. 8C).

Although it has been shown that RNA stabilizes hexameric VP40 in vitro, in this paper, the hexameric VP40 model was constructed in the absence of RNA. The presence of RNA would not significantly alter the overall structure of the hexameric VP40 model, but would necessitate the conformational change of certain residues in order for hexameric VP40 to bind RNA. In the X-ray structure of octameric VP40, side chains of Phe125 and Arg134 of VP40 form strong interactions with the RNA strands; however, because of the absence of RNA, side chains of Phe125 and Arg134 in the hexamer model form residue–residue interactions. As shown in Fig. 8B, the hexameric VP40 model suggests that the aromatic ring of Phe125 forms a cation–π interaction with the side chain amino group of Lys127. Additionally, the side chain of Arg134 forms multiple strong hydrogen bonds. While it may be possible to model the hexameric VP40–RNA complex, the unspecific binding of RNA to hexameric VP40 and the conformational flexibility of the RNA backbone makes modeling the hexamer–RNA complex extremely difficult. However, as shown in Fig. 4, the hexameric VP40 model features large patches of positive electrostatic surface potential at the dimer–dimer interfaces, where RNA could bind nonspecifically and provide additional stability to the protein–protein interfaces as suggested by biochemical data (Timmins et al., 2003a). In contrast, RNA binding in octameric VP40 is specific and plays a structural role in stabilizing the protein–protein interfaces.

3.7. Conformational states of VP40

Besides the monomeric form, VP40 can adopt dimeric, hexameric, and octameric states (Timmins et al., 2003a). Assuming that dimeric VP40 is the building block for both hexameric and octameric VP40, why can VP40 oligomerize into both higher order states? A structural analysis of the hexamer model and the octamer crystal structure reveals that the antiparallel dimers that comprise both structures mostly differ in the spatial separation of their two β-sheets. The degree of twist that can be achieved between the two β-sheets of the N-terminal domain may dictate which of the higher order

states VP40 forms. The centers of the two β-sheets are ~2 Å farther apart in the hexamer model than they are in the octamer crystal structure. This simple conformational switch in the relative position of the two β-sheets of the N-terminal domain may allow VP40 to assume two different oligomeric states and as a corollary, perform multiple functional and structural roles.

4. Conclusion

Although the atomic structure of hexameric VP40 has so far eluded determination, we believe that there is sufficient biochemical and structural data on VP40 to build a reasonable molecular model of the pore-like structure of hexameric VP40. Since hexameric VP40 plays an important role in viral assembly and budding by the Ebola virus, its atomic structure may prove useful in elucidating its function. Here, the two models are presented. The first is an EM reconstruction of truncated hexameric VP40 at ~20 Å and the second is an all-atom model which was fitted to the EM map with a correlation of 0.208. The molecular model indicates that hexamerization involves a major conformational change in the N-terminal domain that is not evident during octamerization.

Acknowledgments

The authors thank the Advanced Biomedical Computing Center at the National Cancer Institute for technical assistance and computing time on the SGI cluster. We also thank Professor Rob Ruigrok for support and discussion. The research described herein was sponsored by the US Army Medical Research and Material Command Research Plan #02-4-3U-057and IAA #Y3-CM-1005-05 (MRMC and NCI) through the OTS Contract #N01-CO-12400. G.S. is supported by the CNRS. The content of this publication does not necessarily reflect the views or policies of the Department of Health and Human Services nor does mention of trade names, commercial products, or organization imply endorsement by the US Government.

References

Aman, M.J., Bosio, C.M., Panchal, R.G., Burnett, J.C., Schmaljohn, A., Bavari, S., 2003. Molecular mechanisms of filovirus cellular trafficking. Microbes Infect. 5, 639–649.

Bavari, S., Bosio, C.M., Wiegand, E., Ruthel, G., Will, A.B., Geisbert, T.W., Hevey, M., Schmaljohn, C., Schmaljohn, A., Aman, M.J., 2002. Lipid raft microdomains: a gateway for compartmentalized trafficking of Ebola and Marburg viruses. J. Exp. Med. 195, 593–602.

Conway, J.F., Steven, A.C., 1999. Methods for reconstructing density maps of "single" particles from cryoelectron micrographs to subnanometer resolution. J. Struct. Biol. 128, 106–118.

Dessen, A., Volchkov, V., Dolnik, O., Klenk, H.D., Weissenhorn, W., 2000. Crystal structure of the matrix protein VP40 from Ebola virus. Embo J. 19, 4228–4236.

Feldmann, H., Jones, S., Klenk, H.D., Schnittler, H.J., 2003. Ebola virus: from discovery to vaccine. Nat. Rev. Immunol. 3, 677–685.

Feldmann, H., Klenk, H.D., 1996. Marburg and Ebola viruses. Adv. Virus Res. 47, 1–52.

Flocco, M.M., Mowbray, S.L., 1994. Planar stacking interactions of arginine and aromatic side-chains in proteins. J. Mol. Biol. 235, 709–717.

Gomis-Ruth, F.X., Dessen, A., Timmins, J., Bracher, A., Kolesnikowa, L., Becker, S., Klenk, H.D., Weissenhorn, W., 2003. The matrix protein VP40 from Ebola virus octamerizes into pore-like structures with specific RNA binding properties. Structure (Camb.) 11, 423–433.

Harty, R.N., Brown, M.E., Wang, G., Huibregtse, J., Hayes, F.P., 2000. A PPxY motif within the VP40 protein of Ebola virus interacts physically and functionally with a ubiquitin ligase: implications for filovirus budding. Proc. Natl. Acad. Sci. USA 97, 13871–13876.

Hoenen, T., Volchkov, V., Kolesnikova, L., Mittler, E., Timmins, J., Ottmann, M., Reynard, O., Becker, S., Weissenhorn, W., 2005. VP40 octamers are essential for Ebola virus replication. J. Virol. 79, 1898–1905.

Jasenosky, L.D., Neumann, G., Lukashevich, I., Kawaoka, Y., 2001. Ebola virus VP40-induced particle formation and association with the lipid bilayer. J. Virol. 75, 5205–5214.

Koradi R., Billeter M., Wuthrich, K., 1996. MOLMOL: a program for display and analysis of macromolecular structures. J. Mol. Graphics 14, 52–55.

Kraulis, P.J., 1991. MOLSCRIPT: A Program to Produce Both Detailed and Schematic Plots of Protein Structures. Journal of Applied Crystallography 24, 946–950.

Laskowski, R.A., MacArthur, M.W., Moss, D.S., Thornton, J.M., 1993. PROCHECK: a program to check the stereochemical quality of protein structures. J. Appl. Crystallogr. 26, 283–291.

Licata, J.M., Simpson-Holley, M., Wright, N.T., Han, Z., Paragas, J., Harty, R.N., 2003. Overlapping motifs (PTAP and PPEY) within the Ebola virus VP40 protein function independently as late budding domains: involvement of host proteins TSG101 and VPS-4. J. Virol. 77, 1812–1819.

Mitchell, J.B., Nandi, C.L., McDonald, I.K., Thornton, J.M., Price, S.L., 1994. Amino/aromatic interactions in proteins: is the evidence stacked against hydrogen bonding?. J. Mol. Biol. 239, 315–331.

Nguyen, T.L., 2004. Three-dimensional model of the pore form of anthrax protective antigen. Structure and biological implications. J. Biomol. Struct. Dyn. 22, 253–266.

Panchal, R.G., Ruthel, G., Kenny, T.A., Kallstrom, G.H., Lane, D., Badie, S.S., Li, L., Bavari, S., Aman, M.J., 2003. In vivo oligomerization and raft localization of Ebola virus protein VP40 during vesicular budding. Proc. Natl. Acad. Sci. USA 100, 15936–15941.

Ruigrok, R.W., Schoehn, G., Dessen, A., Forest, E., Volchkov, V., Dolnik, O., Klenk, H.D., Weissenhorn, W., 2000. Structural characterization and membrane binding properties of the matrix protein VP40 of Ebola virus. J. Mol. Biol. 300, 103–112.

Scianimanico, S., Schoehn, G., Timmins, J., Ruigrok, R.H., Klenk, H.D., Weissenhorn, W., 2000. Membrane association induces a conformational change in the Ebola virus matrix protein. Embo J. 19, 6732–6741.

Timmins, J., Ruigrok, R.W., Weissenhorn, W., 2004. Structural studies on the Ebola virus matrix protein VP40 indicate that matrix proteins of enveloped RNA viruses are analogues but not homologues. FEMS Microbiol. Lett. 233, 179–186.

Timmins, J., Schoehn, G., Kohlhaas, C., Klenk, H.D., Ruigrok, R.W., Weissenhorn, W., 2003a. Oligomerization and polymerization of the filovirus matrix protein VP40. Virology 312, 359–368.

Timmins, J., Schoehn, G., Ricard-Blum, S., Scianimanico, S., Vernet, T., Ruigrok, R.W., Weissenhorn, W., 2003b. Ebola virus matrix protein VP40 interaction with human cellular factors Tsg101 and Nedd4. J. Mol. Biol. 326, 493–502.

Timmins, J., Scianimanico, S., Schoehn, G., Weissenhorn, W., 2001. Vesicular release of ebola virus matrix protein VP40. Virology 283, 1–6.

Wriggers, W., Birmanns, S., 2001. Using situs for flexible and rigid-body fitting of multiresolution single-molecule data. J. Struct. Biol. 133, 193–202.